PERGAMON

Continental Shelf Research 22 (2002) 1379–1395

CONTINENTAL SHELF RESEARCH

www.elsevier.com/locate/csr

The role of topography in small well-mixed bays, with application to the lagoon of Mururoa

Pierre-Philippe Mathieu[a,*], Eric Deleersnijder[b], Benoît Cushman-Roisin[c], Jean-Marie Beckers[d], Karsten Bolding[e]

[a] *Center for Global Atmospheric Modelling, Department of Meteorology, University of Reading, Early Gate, Reading RG6 6BB, UK*
[b] *Institute of Astronomy and Geophysics G. Lemaître, 2 Chemin du Cyclotron Université Catholique de Louvain, B-1348 Louvain-la-Neuve, Belgium*
[c] *Thayer School of Engineering, Dartmouth College 8000 Cummings, Hanover, NH 03755-8000–603/646-3248, USA*
[d] *GeoHydrodynamics and Environment Research Laboratory (GHER), Université de Liège, Sart Tilman B5, B-4000 Liège, Belgium*
[e] *Marine Environment Unit, Joint Research Center (JRC), European Commission, I 21020 Ispra (VA), Italy*

Received 19 July 2000; received in revised form 22 July 2001; accepted 12 September 2001

Abstract

The present study aims to better understand how bathymetry and wind field interact to shape the circulation in well-mixed bays with particular emphasis on the lagoon of Mururoa. The simple model of Csanady (J. Phys. Oceanography 3 (1973) 429) is re-examined and some new analytical properties of the velocity distribution are derived. An extended version of the Csanady model, called the idealised model (IM), is then applied to the lagoon of Mururoa located in the Pacific. The circulation obtained by IM compares well with the circulation simulated by a three-dimensional hydrodynamic model. Our results show that IM provides a simple and powerful heuristic tool to gain more insight into the dominant dynamical regime of the lagoon.

Keywords: Marine modelling; Topographic effect; Idealised hydrodynamic model; Lagoon dynamics; Analytical solution; Tropical pacific; Mururoa atoll lagoon

1. Introduction

Wind-induced currents have been widely acknowledged to play a role of key importance in removing contaminants from various semi-enclosed shallow coastal bays and lagoons (Davies, 1990; Hearn et al., 1987; Hunter and Hearn, 1987; Glorioso and Davies, 1995). A good example is the semi-enclosed lagoon of Mururoa in the tropical Pacific (French Polynesia, 138°55′W–21°50′S), where the wind-induced circulation controls the fate of radioactive substances generated by nuclear weapon tests. The numerical simulations performed by Tartinville et al. (1997) showed that the residence time of radioactive tracers in the lagoon is strongly influenced by the wind-driven barotropic circulation. Namely, the circulation consists of two large gyres which tend to make water re-circulate inside the lagoon rather than to export it toward the open ocean.

Given the key role of wind-driven circulation in pollution study, the present study aims at better

*Corresponding author. Tel.: +44-118-987-5123; fax: +44-118-931-8316.
E-mail address: mathieu@met.rdg.ac.uk (P.-P. Mathieu).

0278-4343/02/$ - see front matter
PII: S0278-4343(02)00002-X

understanding how the effects of wind and bathymetry interact to shape the circulation (i) in shallow homogeneous bays in general and (ii) in the lagoon of Mururoa, in particular. To achieve this objective, we use the simple model of Csanady (1973, 1980) for an infinite channel and extend it for applications to irregular domains of finite extension. This so-called idealised model (IM) is then applied to the lagoon of Mururoa and its results compared with the state-of-the-art general estuarine transport model (GETM) developed by Burchard (1998). Our study builds on the seminal work of Csanady (1973), Simons (1980), Hearn et al. (1987), Glorioso and Davies (1995), Signell et al. (1990), who addressed the role of bottom topography upon circulation in shallow bays. In particular, the results of Csanady (1980) and Hearn et al. (1987) are reviewed and extended (some new properties about the volume transport and velocity are derived). The key point of the present paper is to demonstrate the usefulness of a simplified model approach as a tool to understand dynamical mechanisms in a real flow.

Since the results obtained are based on the simple (although not simplistic) idealised model IM, it is worth stressing the limitations and to keep in mind the assumptions underlying IM when interpreting these results. IM is based on a simplified momentum balance between vertical turbulent shear stress and pressure gradient. Furthermore, for the sake of simplicity in analytical developments, the viscosity is assumed to be constant. This provides a first-order, but obviously crude, approximation of vertical exchange of momentum, since observations and modelling studies indeed show that the vertical viscosity in lakes strongly varies in space and time (Davies, 1990; Davies et al., 2000; Davies and Jones, 1990; Glorioso and Davies, 1995). Given that vertical variation of viscosity are well known to strongly influence the distribution of velocity (Davies, 1990; Glorioso and Davies, 1995; Davies et al., 2000; Davies and Jones, 1990; Signell et al., 1990), one might question the physical basis of using IM to simulate the barotropic circulation in real cases. However, as discussed in Section 4 of the paper, IM despite its strong assumptions has enough complexity to capture the physics necessary to understand the dynamics of Mururoa depth-averaged circulation. In this sense, our process-oriented modelling approach based on a simple model provides a very useful physical complement to the realistic modelling approach of Tartinville et al. (1997) based on a state-of-the-art model.

The paper is structured as follows. In Section 2, we present the IM of Csanady (1973) for the barotropic circulation and investigate the properties of its analytical solution. In Section 3, we illustrate the Csanady "infinite channel" solution for various depth profiles and we then examine how the Csanady solution is affected by the presence of boundaries. In Section 4, we simulate the circulation in Mururoa by use of the three-dimensional numerical model GETM and compare its results with the solution from the idealised barotropic model. Conclusions are drawn in Section 5.

2. Idealised model

In this section, we present the simplified model of Csanady (1973, 1980) and Hunter and Hearn (1987) for the steady-state wind-driven barotropic circulation in a homogeneous basin and derive a streamfunction equation for the barotropic flow. By contrast to these authors, we do not appeal yet to the "infinite channel approximation". The main properties of the analytical solution are derived as in Csanady (1973) and Hunter and Hearn (1987). Namely, Csanady (1973) obtained the analytical expression of the *depth-averaged* velocity showing that the transport is down-wind in the shallow part and up-wind in the deeper part of the infinite channel. Hunter and Hearn (1987) and Hearn et al. (1987) later derived the analytical expression of the *horizontal* velocity and its *variance* for various profiles of vertical eddy viscosity. In particular, they quantified[1] under which conditions a

[1] They define an indicator which measures the relative importance between the "*lateral*" circulation (i.e. variance of the laterally varying depth-averaged velocity) and the "*overturning*" circulation (i.e. variance of the vertically varying horizontal velocity). They obtained an expression of the indicator in terms of the bottom roughness and the depth distribution.

two-dimensional depth-averaged model yields a satisfactory description of the total circulation in a basin. The results of previous studies (Csanady, 1980; Hearn et al., 1987) are then discussed and extended by deriving new properties of the solution and by quantifying how the infinite solution is affected by the presence of boundaries.

2.1. Simplified momentum equations

Following Csanady (1973) for the circulation in a lake, we assumed that the basin is (i) purely wind-driven, (ii) homogeneous (well mixed) and (iii) not influenced by the effects of Earth's rotation (small basin size and Coriolis frequency). With these assumptions, it can be shown, on the basis of scaling arguments, that the horizontal momentum equation governing the steady-state circulation simplifies to a balance between the horizontal pressure gradient (which can be approximated by the sea-surface gradient by use of the hydrostatic equilibrium) and the vertical shear friction. In a Cartesian system of reference (x, y, z) (where the axis z is along the vertical and points upward), the simplified equation for horizontal momentum reads

$$\frac{\partial}{\partial z}\left(\nu\frac{\partial \boldsymbol{u}}{\partial z}\right) - g\nabla_h\eta = 0 \tag{1}$$

and is completed with the following boundary conditions of imposed wind-stress at surface and no-slip condition at bottom

$$\nu\frac{\partial \boldsymbol{u}}{\partial z}\bigg|_{z=0} = \boldsymbol{t}_S \quad \text{and} \quad \boldsymbol{u}|_{z=-H} = 0, \tag{2}$$

where H is the depth, $\boldsymbol{u}$ the horizontal velocity vector, ν the vertical eddy viscosity, η the sea surface elevation relative to a mean state, g the gravity acceleration, ∇_h the horizontal gradient operator and $\boldsymbol{t}_S$ the wind stress vector (normalised by a reference density) in the direction $\boldsymbol{e}_w$. Note that for the rest of the paper, we adopt the convention that vectors are represented in bold characters, while the projection of the vector in the direction of the wind is written in italics (for example, u is the projection of $\boldsymbol{u}$ in the $\boldsymbol{e}_w$ direction).

2.2. Analytical solution

The integration of Eq. (1) requires some assumptions about the vertical variation of the viscosity. In the present paper, the viscosity is assumed constant, although it is known from observations that the viscosity has a strong spatial–temporal variability (Glorioso and Davies, 1995). Using constant viscosity (as opposed to a parabolic profile for example) is motivated by its virtue to enable simple and elegant analytical developments.

By assuming constant viscosity, the analytical solution of Eq. (1) for the velocity reads (Hunter and Hearn, 1987)

$$\boldsymbol{u} = \frac{\boldsymbol{t}_S H}{\nu}\left(\frac{\alpha}{2}\sigma^2 + \sigma(1-\alpha)\right), \tag{3}$$

where the dimensionless depth σ and dynamical ratio α are defined as follows:

$$0 \leqslant \sigma \equiv 1 + \frac{z}{H} \leqslant 1 \tag{4}$$

and,

$$\alpha(x, y) \equiv \frac{Hg\nabla_h\eta \cdot \boldsymbol{e}_w}{\boldsymbol{t}_S \cdot \boldsymbol{e}_w} = \frac{\text{Pressure gradient}}{\text{Wind friction}}. \tag{5}$$

The parameter α (varying horizontally) plays a key role in determining the dynamical regime since it measures the subtle balance between counter forces generating two types of currents:

- *Wind drift current* (down-wind) directly generated by wind.
- *Gradient current* (up-wind) resulting from the change in sea surface elevation (induced indirectly by wind via piling up of water along the coast).

An analytical expression for the transport can be obtained by integrating vertically Eq. (3)

$$U \equiv \int_{-H}^{0} \boldsymbol{u}\,\mathrm{d}z = \frac{\boldsymbol{t}_S H^2}{\nu}\left(\frac{1}{2} - \frac{1}{3}\alpha\right). \tag{6}$$

The bottom stress can be derived by taking the vertical derivative of Eq. (3) or by integrating Eq. (1) along the vertical

$$\boldsymbol{t}_B \equiv \nu\frac{\partial \boldsymbol{u}}{\partial z}\bigg|_{z=-H} = \boldsymbol{t}_S(1-\alpha) \tag{7}$$

and expressed in terms of the transport and pressure gradient by use of Eqs. (5) and (6)

$$\boldsymbol{t}_B = \frac{2\nu}{H^2}\boldsymbol{U} - \frac{gH}{3}\nabla_h\eta. \tag{8}$$

In our simplified model, the bottom stress depends linearly on the transport and the pressure gradient while, in reality, the bottom stress should depend on bottom surface properties and boundary layer flow. This simplicity of the bottom stress formulation results directly from the assumption of constant viscosity and will be the key to the development of the IM in Section 2.4.

2.3. Flow properties

In this section, we examine the key properties of the analytical solution that are summarised in the $\alpha-\sigma$ graphic of Fig. 1. These properties are similar but more general than in the work of Csanady (1980) because we do not appeal to the infinite channel approximation. Three main dynamical regimes are distinguished:

- $\alpha<1$.
- The horizontal velocity is down-wind over the whole water column (e.g. the surface velocity is $u = t_S H/\nu(1-\alpha/2) > 0$). This regime corresponds for example to a shallow region of the bay where the direct effect of wind is dominant.
- $1\leqslant\alpha\leqslant 2$.

  The horizontal velocity reverses its direction along the vertical. It vanishes along a reversal surface Γ of equation $\sigma(x,y) = 2(1-1/\alpha)$ which intersects the bottom at $\alpha = 1$ and outcrops at surface at $\alpha = 2$.
- $\alpha > 2$.

  The horizontal velocity is up-wind over the whole water column (e.g. the surface velocity is $u = t_S H/\nu(1-\alpha/2) < 0$). This regime corresponds for example to the deep region of the bay where the indirect effect of wind is dominant.

Some particular values of α are of interest:

- $\alpha = \frac{3}{2}$.

  The transport vanishes and reverses from a down-wind direction (in the shallow region) to a up-wind direction (in the deeper region of the domain), as previously shown by Csanady (1973)
- $\alpha = 1$.

  The bottom stress vanishes. It is worth stressing that, outside the range $1<\alpha<3/2$, the dynamical balance is such that the bottom stress is in the same direction as the transport.

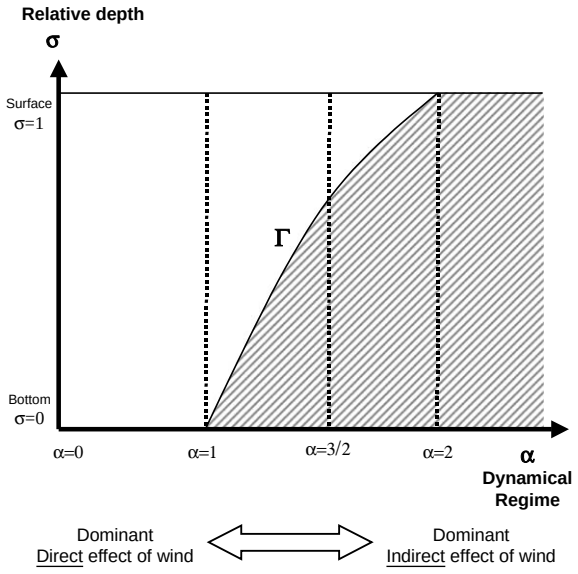

Fig. 1. Representation in the $\sigma-\alpha$ plane of the properties of the analytical solution of the IM Eq. (1). The reversal surface Γ separates the regime where the velocity is down-wind from the region where the velocity is up-wind (hatched region).

2.4. Idealised model

In this section, we derive an equation (based on Eq. (1), the simplified momentum equation) governing the distribution of the steady-state depth-averaged circulation in a closed basin. This is achieved by applying the curl operator $\nabla_h\wedge$ to the barotropic transport Eq. (7) in order to eliminate the pressure gradient

$$\nabla_h\wedge\left(\frac{\boldsymbol{t}_S-\boldsymbol{t}_B}{H}\right) = 0. \tag{9}$$

Let us define a streamfunction for a steady-state non-divergent flow such that

$$\frac{\partial U^x}{\partial x}+\frac{\partial U^y}{\partial y} = 0 \Rightarrow (U^x, U^y) \equiv \left(\frac{\partial\psi}{\partial y}, -\frac{\partial\psi}{\partial x}\right). \tag{10}$$

By combining Eqs. (8)–(10), we obtain the equation governing the streamfunction

$$\frac{\partial}{\partial x}\left(\frac{2\nu\,\partial\psi}{H^3\partial x}\right)+\frac{\partial}{\partial y}\left(\frac{2\nu\,\partial\psi}{H^3\partial y}\right)+\frac{\partial}{\partial x}\left(\frac{t_S^y}{H}\right)-\frac{\partial}{\partial y}\left(\frac{t_S^x}{H}\right)=0. \tag{11}$$

The above equation will be referred to as the IM for the rest of the paper. It enables to study the effects of bathymetry in a basin of arbitrary geometry. To the best of our knowledge, IM has not been derived in previous studies and constitutes, thereby, a useful extension of the model of Csanady (which was only valid for an infinite channel) and complements the work of Hunter and Hearn (1987) by investigating the role of bathymetry in various basins of finite extension. Within this paper, IM will be used to study the circulation analytically, in a rectangular basin (Section 3), and numerically, in the lagoon of Mururoa (Section 4).

3. Idealised geometry and bathymetry

Within this section, we illustrate the behaviour of the analytical solution of Eq. (1) by restricting the discussion to an idealised geometry. Firstly, we consider a channel of infinite length, as done previously by Csanady (1973) and Hearn et al. (1987). We illustrate the Csanady solution for various channel bathymetry and derive some original properties of the transport of mass and how the transport reverses. Secondly, we consider a rectangular basin to investigate the effects of boundaries on the infinite channel solution extending, thereby, the results of Csanady (1973) and Hearn et al. (1987).

3.1. Infinite channel

Following Csanady (1973) and Hunter and Hearn (1987), we assume that (i) the domain is a channel with an infinite length in the direction x and a width of "2 L_y" in the direction y, (ii) the wind blows in the direction x with a constant magnitude, (iii) the depth varies in the direction y, (iv) the net flow through the channel is zero

$$\int_0^1\int_{-L_y}^{+L_y} u\,\mathrm{d}y\,\mathrm{d}\sigma=0. \tag{12}$$

By inserting the velocity expression (Eq. (3)) into Eq. (12), we obtain the following momentum equation, where the bottom stress has been included in the pressure gradient term

$$t_S-\frac{2}{3}g\,H_*\frac{\mathrm{d}\eta}{\mathrm{d}x}=0, \tag{13}$$

where H_* is the inversion depth (corresponding to the depth where the barotropic transport reverts direction) defined as follows:

$$H_*=\frac{\overline{H^3}}{\overline{H^2}} \tag{14}$$

in terms of the statistical n-moments of depth (where overbar refers to the average operator in the direction y),

$$\overline{H^n}\equiv\frac{1}{2L_y}\int_{-L_y}^{+L_y}H^n\,\mathrm{d}y. \tag{15}$$

By virtue of our assumption of an infinite channel, the parameter α can now be explicitly expressed as a simple re-scaling of the depth profile

$$\alpha(y)=\frac{3\,H}{2H_*}. \tag{16}$$

3.1.1. Specific properties

Some new properties of the dynamical fields in an infinite channel are derived. For reasons of convenience and clarity, the variables are written in dimensionless form. It is worth recalling that the properties derived below depend on our assumption of constant viscosity. They should only be considered as a guide to provide a first guess of how the flow behaves for various bathymetry (where it becomes maximal and reverses).

3.1.1.1. Velocity. The dimensionless velocity reads:

$$u'\equiv\frac{\nu}{t_S H_*}u=\sigma\frac{H}{H_*}\left(\frac{3}{4}\sigma\frac{H}{H_*}-\frac{3}{2}\frac{H}{H_*}+1\right). \tag{17}$$

It vanishes along the line of equation $z = H - 4/3\,H_*$ and has the following interesting properties:

- $u'|_{\sigma=1} = \dfrac{H}{H_*}\left(1 - \dfrac{3\,H}{4H_*}\right)$. (18)

  The velocity at the surface is opposed to the wind direction only if the maximal depth is higher than $4/3\,H_*$ (Fig. 2)

- $u'_{\max} = u'|_{\sigma=1,H=2/3H_*} = \dfrac{1}{3}$. (19)

  The largest down-wind velocity ($u' = +1/3$) is found at surface at a horizontal position just above the point where the separation surface Γ intersects the bottom (Fig. 2)

- $u'_{\min} = u'|_{\sigma=(\alpha_m-1)/\alpha_m,H=H_m} = -\dfrac{1}{3}\left(\dfrac{3}{2}\dfrac{H_m}{H_*} - 1\right)^2$. (20)

  The largest up-wind velocity ($u' < 0$) is found at the equivalent depth ($z = -H_*$) at a horizontal position where the depth is maximal as illustrated in Fig. 2.

3.1.1.2. Transport and streamfunction. Using Eq. (16), the depth-averaged velocity Eq. (6) can be rewritten in the following dimensionless form:

$$U' \equiv \frac{v}{t_S H_*^2}\,U = \frac{1}{2}\left(\frac{H}{H_*}\right)^2\left(1 - \frac{H}{H_*}\right) \tag{21}$$

and has the following properties:

- $U'_{\text{flat}} = U'|_{H=H_*} = 0$. (22)

  In a basin with flat bottom (the depth equals H_* everywhere), the horizontal velocity adjusts on the vertical in such a way that the transport is zero

- $U'_{\max} = U'|_{H=2/3H_*} = \dfrac{2}{27}$. (23)

  The largest down-wind transport is found at the same position as the maximal velocity (Fig. 2)

- $H_* \geqslant \bar{H}$. (24)

  This geometrical property demonstrated in Appendix A states that the inversion depth for the transport is always deeper than the mean depth. This extends the results of Csanady (1980) who showed that, in the absence of bottom friction, the inversion of the flow occurs at the mean depth. Our results suggest, therefore, that the effect of bottom friction is to deepen the inversion depth, thereby widening the region of up-wind transport.

3.1.1.3. Directional volume transport. Let us define the dimensionless directional mass transport as

$$Q' \equiv \frac{1}{2L_y}\int_{-L_y}^{+L_y} U'_-\,\mathrm{d}y, \tag{25}$$

where U'_- is the dimensionless vertical transport in the up-wind direction obtained by integrating the horizontal velocity only in the region where it is up-wind (hatched surface represented in Fig. 1),

$$U'_- \equiv \frac{v}{t_S H_*^2}\int_0^{\Gamma(z)} u\,\mathrm{d}z = \frac{H}{H_*}\int_0^{\Gamma(\sigma)} u'\,\mathrm{d}z. \tag{26}$$

Note that the up-wind volume transport equals the down-wind volume transport by virtue of Eq. (12). By injecting Eq. (17) in Eq. (26), we obtain an expression of U'_- (three different dynamical regions are distinguished because the limits of the vertical integral in Eq. (26) depend on the horizontal position)

$$U'_- = \begin{cases} 0 & \text{for} \quad H < \dfrac{2}{3}H_*, \\ \dfrac{8}{27}\left(\dfrac{3\,H}{2H_*} - 1\right)^3 & \text{for} \quad \dfrac{2}{3}H_* \leqslant H \leqslant \dfrac{4}{3}H_*, \\ \dfrac{1}{2}\left(\dfrac{H}{H_*}\right)^2\left(\dfrac{H}{H_*} - 1\right) & \text{for} \quad H > \dfrac{4}{3}H_*. \end{cases} \tag{27}$$

A dimensionless measure of the directional volume transport per unit of cross-sectional surface S' can be obtained as follows:

$$q' \equiv \frac{Q'}{S'^2} \text{ with } S' \equiv \frac{1}{2L_y}\int_{-L_y}^{+L_y}\frac{H}{H_*}\,\mathrm{d}y. \tag{28}$$

This quantity has some interesting properties, which have not been discussed in previous studies

- $q'_{\text{flat}} = q'|_{H=H_*} = \dfrac{1}{27}$. (29)

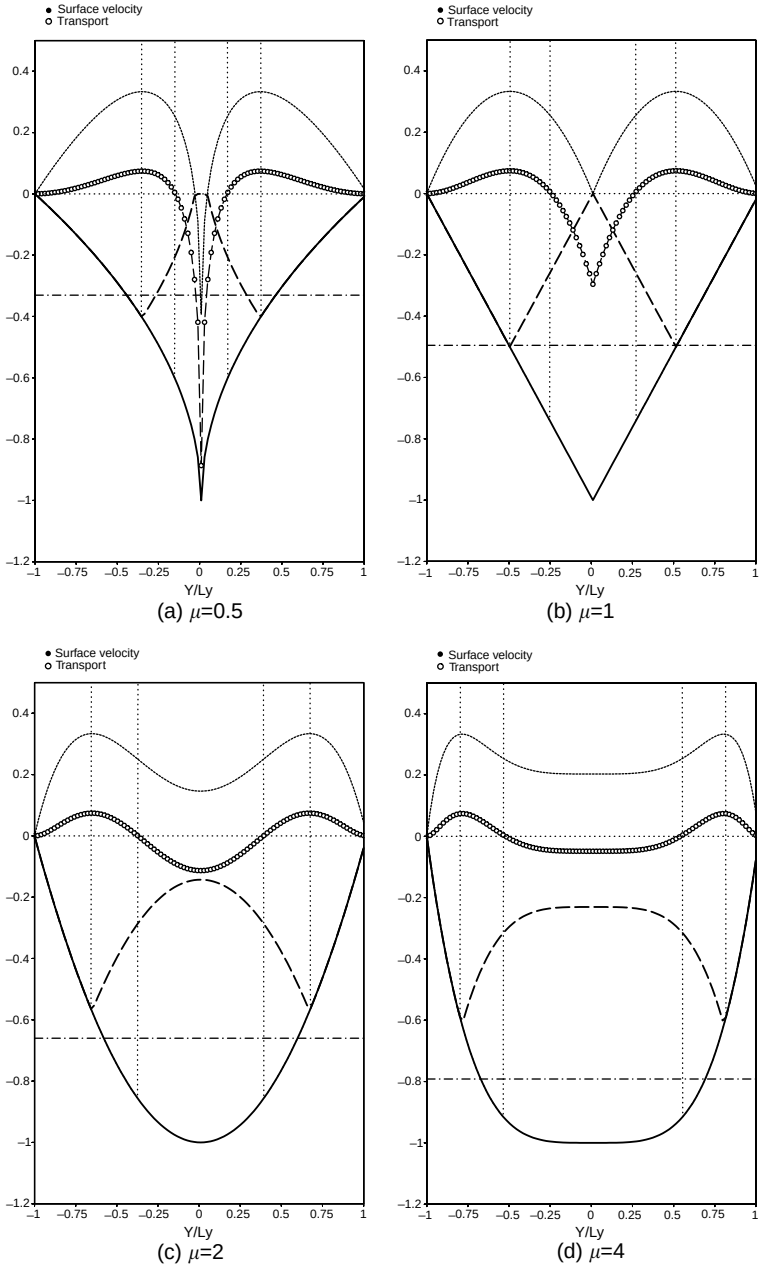

Fig. 2. Analytical solution for the infinite channel for various values of the slope parameter μ (defined in Eq. (31)). The various lines represent the depth profile (solid line), the reversal surface Γ (bold long dashed line), the dimensionless surface velocity (dotted line), and the dimensionless barotropic transport (empty circle). The horizontal line represents the mean depth (long dashed dotted) and the vertical lines correspond to $\alpha = 1$ and $3/2$.

By using $H = H_*$ in Eq. (28), it is seen that q' equals 1/27 in a flat bottom channel

- $$\frac{1}{27}\frac{\overline{H^2}}{\bar{H}^2} \leqslant q' \leqslant -\frac{13}{24} + \frac{169}{432}\left(\frac{\bar{H}}{H_*}\right)^{-2} + \frac{3}{16}\frac{\overline{H^2}}{\bar{H}^2}. \quad (30)$$

As demonstrated in Appendix A and illustrated in Fig. 3, the directional flux per square unit area is bounded by the above expressions. By virtue of the Schwartz inequality $\overline{H^2} \geqslant \bar{H}^2$, it is readily seen that q' is always larger than the transport in a flat channel. This illustrates the role of bathymetry by showing that a sloping bottom enables higher transport than a flat bottom for the same cross-section.

3.1.2. Applications for various depth profiles

In order to illustrate graphically the properties of the analytical solution, we assume the following generic polynomial form of a symmetric depth profile:

$$\frac{H}{\bar{H}} = \frac{\mu+1}{\mu}\left(1 - \left|\frac{y}{L_y}\right|^{\mu}\right), \quad (31)$$

where the parameter $\mu \geqslant 0$ is a measure of bottom slope (for $\mu = 1$, the profile is linear and for higher μ, the section tends to a rectangle). With such a profile, we have the following geometrical properties:

$$\left(\frac{\overline{H^2}}{\bar{H}^2}, \frac{\overline{H^3}}{\bar{H}^3}\right) = \left(\frac{2\mu+2}{(2\mu+1)}, \frac{6(\mu+1)^2}{(3\mu+1)(2\mu+1)}\right) \quad (32)$$

such that:

$$\alpha(y) = \frac{3\mu+1}{2\mu}\left(1 - \left|\frac{y}{L_y}\right|^{\mu}\right). \quad (33)$$

The various properties of the transport and surface velocity (extreme, reversal surface) are illustrated in Fig. 2 for a variety of bottom profiles.

It is shown that for higher values of μ:

- The barotropic transport weakens, tending to a value of zero for a flat bottom channel.
- The region of down-wind transport narrows, tending to a jet for very steep bathymetry.
- The separation surface Γ moves toward the bottom (note that the separation surface only outcrops at the surface for a convex depth profile with $\mu \leqslant 1$ such as in Fig. 2a.
- The directional transport weakens, tending to a value of 1/27 for a flat bottom channel (Fig. 3).

3.2. Rectangular basin

In this section, we investigate how the "long-basin" analytical solution for transport is influenced by the presence of boundaries. We consider a rectangular basin where the depth varies only in the y-direction and the wind blows in the x-direction. With such assumptions, the IM streamfunction equation (Eq. 11) simplifies to

$$\delta^2\frac{\partial^2\psi'}{\partial x'^2} + H'^3\frac{\partial}{\partial y'}\left(\frac{1}{H'^3}\frac{\partial\psi'}{\partial y'}\right) + H'\frac{\mathrm{d}H}{\mathrm{d}y'} = 0 \quad (34)$$

expressed in terms of the following dimensionless variables:

$$(x',\, y',\, H',\, \delta,\, \psi') \equiv \left(\frac{x}{L_x}, \frac{y}{L_y}, \frac{H}{H_*}, \frac{L_y}{L_x}, \frac{2v\psi}{L_y H_*^2 t_S}\right). \quad (35)$$

In order to solve Eq. (34), we derive first the expression of the infinite channel streamfunction "ψ'_∞" solution of the following equation (using $\delta = 0$ in Eq. (34)):

$$\frac{\partial}{\partial y'}\left(\frac{1}{H'^3}\frac{\partial\psi'_\infty}{\partial y'}\right) + \frac{1}{H'^2}\frac{\mathrm{d}H}{\mathrm{d}y'} = 0. \quad (36)$$

The solution of Eq. (36) can be directly derived by integrating Eq. (21). However, it is convenient to write it as a series of functions $Y_n(y')$ modulated by a coefficient χ_n,

$$\psi'_\infty = \sum_{n=0}^{\infty} \chi_n Y_n(y'). \quad (37)$$

The functions $Y_n(y')$ are chosen to be solution of the following eigenvalue problem:

$$\frac{\mathrm{d}}{\mathrm{d}y'}\left(\frac{1}{H'^3}\frac{\mathrm{d}Y_n}{\mathrm{d}y'}\right) + \frac{\lambda_n}{H'^3}Y_n = 0 \quad \text{with} \quad Y_n(y' = \pm 1) = 0 \quad (38)$$

and normalised as follows:

$$\int_{-1}^{+1} \frac{Y_n^2}{H'^3}\,\mathrm{d}y' = 1. \quad (39)$$

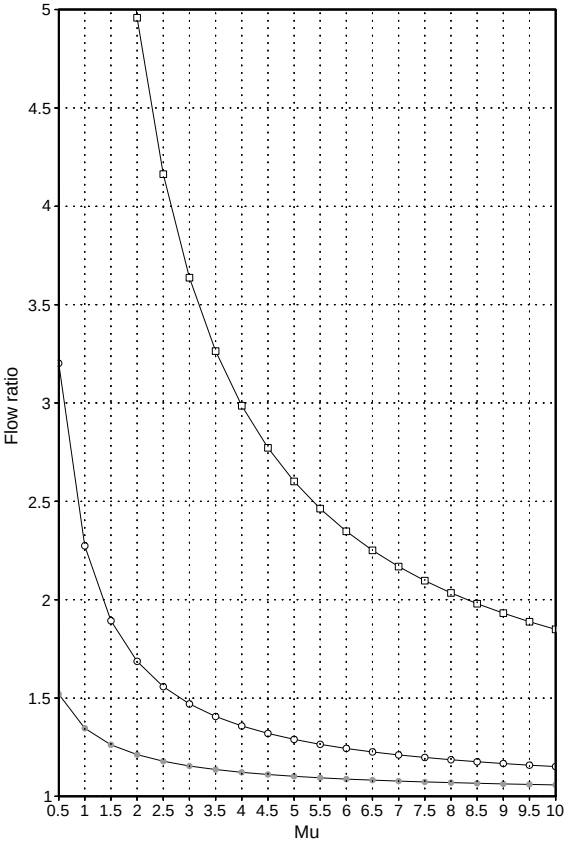

Fig. 3. Evolution of the directional transport per square unit area (q' is defined in Eq. (28) and represented by empty circles), its lower bound (represented by solid circles) and its upper bound (represented by empty squares) versus the slope parameter (μ defined in Eq. (31)). All quantities are normalised by 1/27 that is the value of the directional transport in a flat channel.

The eigenfunctions verifies the property of orthogonality

$$\int_{-1}^{+1} \frac{Y_m Y_n}{H^{3'}}\,\mathrm{d}y' = 0 \ \text{ for } m \neq n. \tag{40}$$

By using Eqs. (39) and (40) in Eq. (38), it can be shown that the weighing coefficients are the projection of the infinite solution on the base of eigenfunctions

$$\chi_n = \int_{-1}^{+1} \frac{Y_n \psi'_\infty}{H'^3}\,\mathrm{d}y'. \tag{41}$$

An explicit expression of the weighing coefficient in terms of the eigenfunctions and the bathymetry is obtained by replacing ψ'_∞ in Eq. (36) using its definition Eq. (37) and integrating by part

$$\chi_n = \frac{1}{\lambda_n} \int_{-1}^{+1} \frac{Y_n\,\mathrm{d}H'}{H'^2\,\mathrm{d}y'}\,\mathrm{d}y'. \tag{42}$$

As the eigenfunctions and weighing coefficients are known, we now look for a solution of Eq. (34) in the following form (similar to ψ'_∞ but with a dependency on the direction x):

$$\psi' = \sum_{n=0}^{\infty} \chi_n X_n(x')\, Y_n(y'). \tag{43}$$

Substituting Eq. (43) into Eq. (34) and using the property of Eqs. (39)–(40), we obtain the equation governing the functions $X_n(x')$

$$\delta_n^2 \frac{\mathrm{d}^2 X_n}{\mathrm{d}x'^2} - X_n + 1 = 0 \ \text{ with } X_n(x' = \pm 1) = 0, \tag{44}$$

where the parameter δ_n is defined to be

$$\delta_n = \frac{\delta}{\sqrt{\lambda_n}}. \tag{45}$$

The solution of Eq. (44) reads

$$X_n(x') = 1 - \frac{\cosh(x'/\delta_n)}{\cosh(1/\delta_n)}. \tag{46}$$

The above function is represented in Fig. 4 for various values of δ_n showing that it is almost everywhere equal to 1 except in a thin boundary layer where it rapidly decreases to zero.

The solution Eq. (43) is depicted in Fig. 4a for a rectangular basin with a quadratic depth profile. It illustrates that the solution for an aspect ratio of $\delta = 1/2$ is close to the solution for an infinite channel $\delta = 0$ except in the boundary layer in the ends of the basin. The damping of the streamfunction near boundaries is illustrated in Fig. 4a and b. It corresponds to the infinite channel solution weighted by the functions represented in Fig. 4d. A transect of dimensionless horizontal velocity is displayed in Fig. 4c to illustrate the reversal of velocity along the vertical in the deep region of the basin and a down-wind velocity in the shallow region.

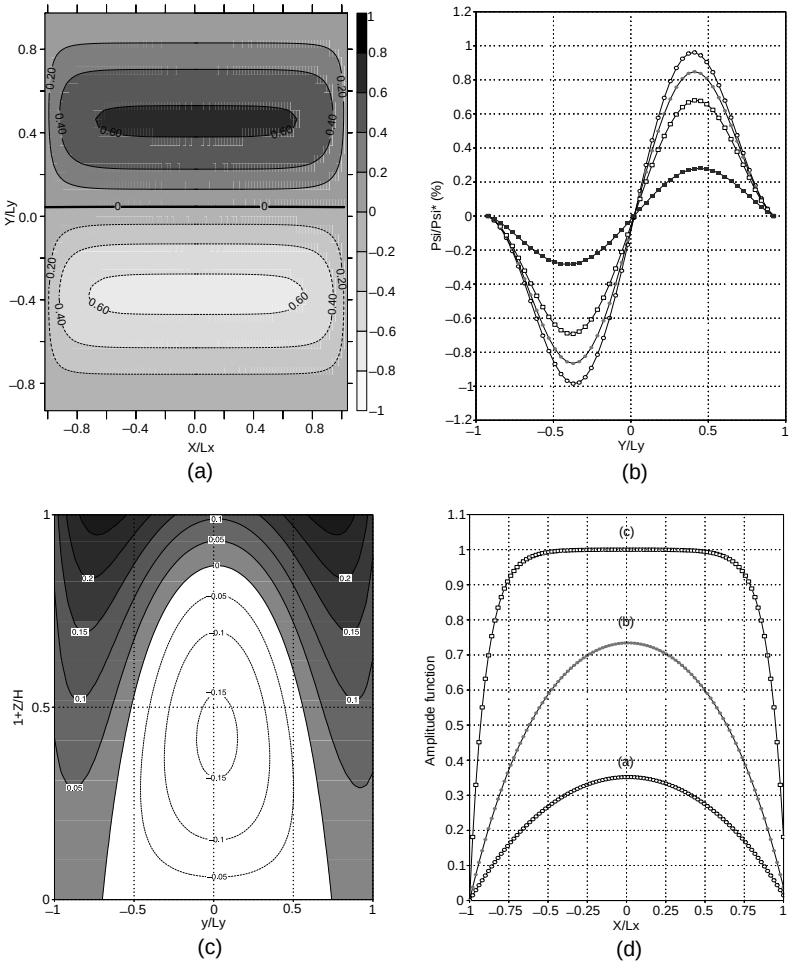

Fig. 4. (a) Pattern of normalised horizontal streamfunction ψ/ψ_* (in %) obtained by IM applied to a rectangular basin (with a parabolic profile of depth and an aspect ratio of $\delta \cong 1/2$) and forced by a constant westward wind stress, (b) sections of this normalised streamfunction at $x/L_x = 10\%$ (empty circle), $x/L_x = 20\%$ (solid circle), $x/L_x = 30\%$ (empty square) and $x/L_x = 80\%$ (solid square). (c) transect of dimensionless velocity in sigma co-ordinate computed from Eq. (3). (d) Shape function "$X(x)$" (defined in Eq. (46)) for various values of the aspect ratio parameter: (a) $\delta_n = 1$, (b) $\delta_n = 1/2$ and (c) $\delta_n = 1/10$.

4. Application to realistic case: the lagoon of Mururoa

In this section, we use (i) the simple model IM and (ii) the sophisticated three-dimensional hydrodynamic model GETM to simulate the barotropic circulation in the lagoon of Mururoa. There is a difficulty in comparing both models because they have different boundary conditions at the bottom: IM is based on a no-slip boundary condition (associated with a linear bottom stress) while GETM uses a quadratic bottom stress. In order to perform a sensible comparison of model outputs, we adjust the viscosity in IM (which is the only free parameter) such that the elevation pattern in each simulation is similar.

4.1. Key oceanographic features in the lagoon Mururoa

The lagoon of Mururoa is a small semi-enclosed body of water ($25\,\text{km} \times 10\,\text{km}$) with a small

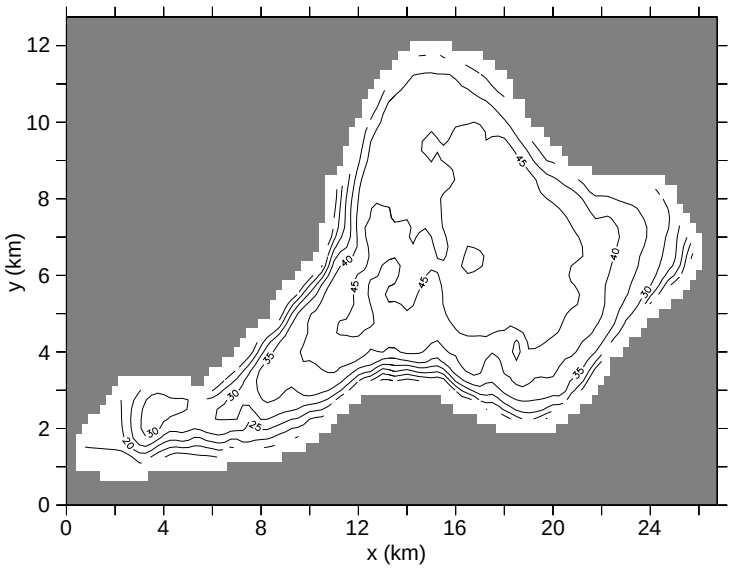

Fig. 5. Bathymetry of the lagoon of Mururoa (depth in m) characterised by a wide and deep basin in its eastern part (maximal depth of 55 m) and a very narrow and shallow basin in its western part. The lagoon is connected with the Pacific in its western part via a large (2 km wide) and shallow (8 m depth) pass ($x = 10$ km, $y = 6-8$ km). Due to a rather low elevation (3 m average height), the atoll rim (65 km length, 100 m width) can be submerged by Pacific water in some regions called hoas and located in the Southern reef.

connection to the Pacific on its western side (see Fig 5). Due to its particular oceanographic features described hereafter, the lagoon appears particularly suited to demonstrate the usefulness of the IM because its dynamics is likely to be dominated by a simple balance between friction and pressure gradient (Tartinville, 1998) as in IM.

The main oceanographic features of the basin are:

- "The wind stress is the main driving force for the long-term circulation in the Mururoa lagoon" as concluded by Tartinville et al. (1997) who explored the sensitivity of the Mururoa lagoon circulation to the forcing of wind, tides and the overflows over the so-called hoas (regions where Pacific water submerge the reef).
- The semi-diurnal tidal M_2 tide entering through the pass was shown by Tartinville et al. (1997) to weakly influence the barotropic circulation.
- The effects of stratification are negligible in the momentum equation. As shown by the hydrological observations of Rancher (1995), the lagoon is quasi-homogeneous and the buoyancy term can be reasonably neglected. Since the lagoon is shallow and its water acts as a single density layer, the effects of bathymetry on the circulation are likely to be important.
- The effects of the Earth's rotation are a priori very weak due to the small dimensions of the basin and the proximity of the equator (21°50'S). This is confirmed by a scaling analysis of the Coriolis term and has been verified by our numerical tests (not shown here).

4.2. Hydrodynamic model set-up

The hydrodynamic model GETM of Burchard (1998) is based on the primitive equations (Bryan, 1969) expressed in sigma co-ordinate. The vertical viscosity is computed by a realistic second-order turbulence closure (Mellor and Yamada, 1982). The bottom stress is computed as a quadratic function of the velocity in the grid box adjacent to the seabed (Blumberg and Mellor, 1987). The drag coefficient includes the bottom roughness length,

which is set to 0.04 m, according to Black (1993) and Tartinville et al. (1997). The grid resolution is 250 m × 250 m (108 × 52 grid points) in the horizontal plane and 15 sigma levels along the vertical.

The GETM simulations are performed by assuming that Mururoa is a closed lagoon (no pass) and forced by a constant wind of 0.1 N/m^2 roughly corresponding to the dominant trade wind of 10 m/s blowing westward (Bourlat et al., 1995). These approximations are reasonable regarding the weak influence of tidal forcing on the long-term wind-driven barotropic circulation (Tartinville et al., 1997; Deleersnijder et al., 1997) and our focus on the investigation of wind–bathymetry interactions.

4.3. Simulation of the circulation

An analysis of the different terms of the momentum equation in the hydrodynamic model has revealed that the dynamics of the lagoon is mainly controlled by a balance between the friction terms and the pressure gradient. The wind-driven barotropic circulation is depicted in Fig. 6 for various model runs: (a) IM, (b) GETM without advection, (c) GETM with non-linear advective effects and (d) GETM without advection applied to a *flat* basin. A more qualitative comparison of the various runs is provided in Fig. 7, which represents the dimensionless streamfunction for the infinite channel solution, IM and GETM in several sections.

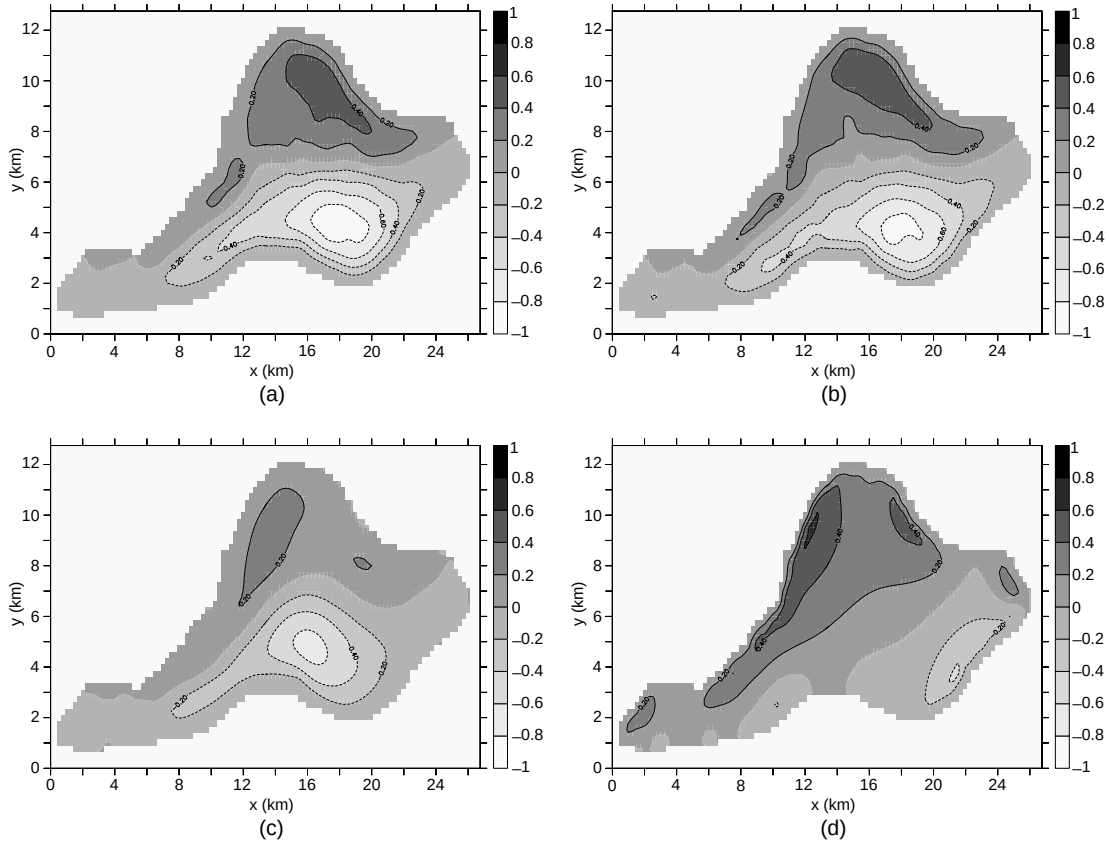

Fig. 6. Horizontal circulation in Mururoa. Normalised streamfunction ψ/ψ_* (in %) for the (a) analytical solution from IM, (b) GETM solution without advection, (c) GETM solution with advection, (d) GETM without advection and for a flat bathymetry. Note that in (d) the dimensionless streamfunction has been multiplied by a factor 400.

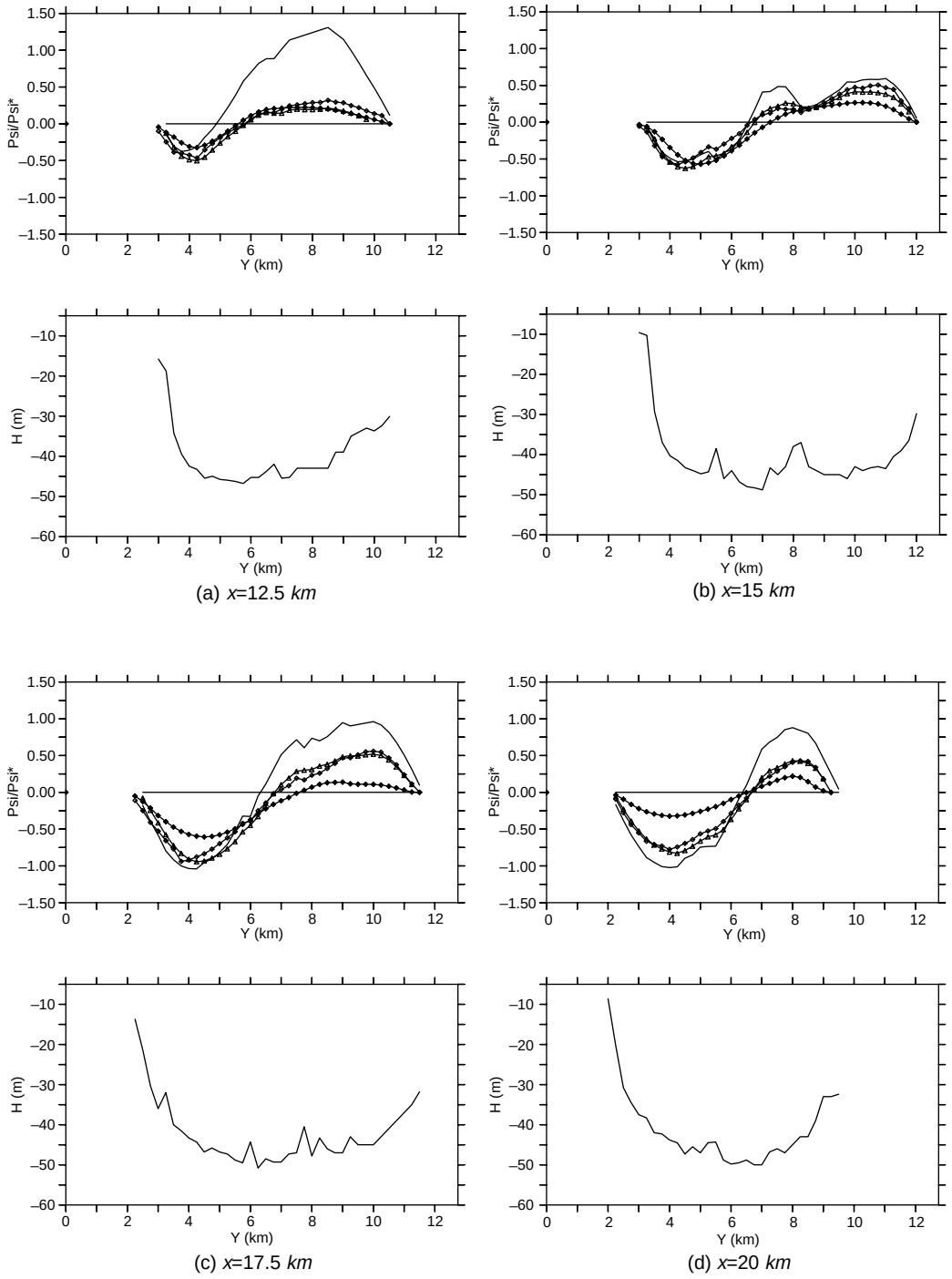

Fig. 7. Longitudinal sections of normalised streamfunction ψ/ψ_* in (%) (upper panel) and associated bathymetry profile (lower panel). The streamfunction is represented for the analytical solution for the infinite channel (solid line), the IM (empty triangle), the hydrodynamic model without advection (empty diamond) and the hydrodynamic model solution with advection (solid diamond). The position of the sections (a) $x = 12.5$ km, (b) $x = 15$ km, (c) $x = 17.5$ km and (d) $x = 20$ km.

Figs. 6a–c correspond to the circulation simulated with a realistic bathymetry. They all present a similar pattern of circulation consistent with observations (Rancher, 1995) and previous modelling study (Tartinville, 1998): two gyres with a down-wind current in the shallow part and a returning up-wind current in the deeper part. The region where the velocity is down-wind is very close to the coast because of the steepness of the bathymetry in Mururoa.

The two-cells circulation pattern is mainly controlled by the balance between wind stress and sea-surface elevation force as follows: (i) the wind blows from the East entraining surface water towards the West, (ii) the moving water piles up on the western coast, thereby inducing a surface-slope pressure gradient which, in turn, tends to create an up-wind current. The depth-averaged circulation, therefore, results from a simple balance between (i) the "direct effect of wind" through friction (dominant in the shallow part) and (ii) the "indirect effect of wind" via the sea-surface pressure gradient (dominant in the deeper part). This circulation is in agreement with the results obtained on idealised test cases.

The comparison of Fig. 6a and b demonstrates that the solution of IM is in good agreement with the GETM simulation performed without advection. Fig. 7 further supports this point and clearly shows that IM performs better than the infinite channel streamfunction, which is too strong (consistent with our analytical results in the rectangular basin) and does not reverse at the right position. This suggests that the simple model IM includes the necessary physics to produce a first realistic guess of the barotropic circulation in Mururoa. The good agreement between IM and GETM might look surprising given the differences of bottom boundary condition and viscosity profile between the simple model (no-slip condition, constant viscosity in IM) and sophisticated model (quadratic bottom stress, parabolic-like viscosity in GETM). However, given our focus on barotropic circulation (less sensitive to viscosity profile) and in the particular case of Mururoa (well mixed), this similarity of behaviour can be understood. Indeed, even if the vertical distribution of the horizontal velocity (baroclinic circulation) is clearly strongly sensitive to the profile of viscosity, the horizontal distribution of the depth-averaged velocity (barotropic circulation) is more likely to be controlled by the balance between wind stress, sea-surface gradient and bottom stress. In our case, the wind stress is constant and the patterns of sea surface elevation in both models are made similar by tuning the viscosity in IM. Consequently, the horizontal depth-averaged circulation is mainly influenced by the viscosity only through the bottom stress. In the lagoon of Mururoa, the hydrodynamical conditions appear to be such that the different bottom boundary conditions and viscosity profiles of IM and GETM actually do qualitatively similar jobs. However, this similarity of behaviour should be taken with caution when applied to other domains or dynamical regimes.

The comparison of Fig. 6b and c illustrates clearly the effect of advection. It is shown that advection of momentum (non-linear effect) does not affect qualitatively the circulation pattern but weakens and smoothes the streamfunction. This results mainly from the spurious implicit diffusivity of the upstream advective scheme we use and is further quantitatively illustrated in Fig. 7.

The comparison of Fig. 6b and d illustrates the critical role of bathymetry in shaping the circulation. Although both runs have similar patterns of sea-surface pressure gradient (because the wind piles up water on the Western coast in each simulation), they have a totally different type of barotropic circulation due to their different bathymetry. In fact, the barotropic transport should be, in theory, zero in a flat basin (see Eq. (11)) but GETM creates, via boundary effects, a very weak residual circulation including several sluggish cells (note the scaling factor of 40 in the magnitude).

5. Conclusions

The main goal of the present paper is to use a simple but physical modelling approach to better understand the influence of bathymetry on the circulation in a shallow homogeneous basin. To do that, we have used the simple model of Csanady (1973) (for a wind-driven, barotropic

and non-rotational flow in an infinitely long channel), extended its results and applied it on various analytical test cases (infinite channel, rectangular basin) as well as on one real application (lagoon of Mururoa). Our objective has been pursued in three steps.

Firstly, the properties of the Csanady (1973) model for a constant viscosity have been reviewed and some original properties of the flow have been derived. In particular, we have investigated how the effects of wind stress, pressure gradient and bathymetry combine to shape the *vertical* distribution of horizontal velocity in an infinite channel (position where velocity is maximum, minimum and reverses). Simple examples have been used to illustrate how the bottom slope determines the pattern of reversal of velocity. An interesting result is that a sloping bottom always provides a higher volume transport per unit area than a flat bottom.

Secondly, the Csanady model has been generalised to be applied to a basin of finite size. A streamfunction equation (so-called Idealised Model—IM) governing the barotropic flow in the *horizontal* plane has been derived. An analytical solution of this model has been derived for a rectangular basin showing that borders affect the solution of the infinite channel model only in the lateral boundary layers.

Thirdly, the physical relevance of the IM has been assessed in more complex geometrical frameworks by applying it to the lagoon of Mururoa to simulate the barotropic circulation. The IM has been shown to provide a realistic pattern of barotropic circulation, which is in good agreement with the circulation obtained by a fully three-dimensional hydrodynamic model GETM (run without advection).

Two key virtues of IM have been demonstrated in this modelling exercise: (i) IM is a simple tool which helps to gain insight into the dynamics of the circulation in Mururoa, (ii) IM provides a first guess of the double gyre barotropic circulation in Mururoa without the need to run a three-dimension model. IM thereby appears as a cheap option to investigate the sensitivity of the Mururoa circulation to changes in wind stress pattern and, therefore, to shed some light on the transport of radioactive tracers.

In conclusion, the simple modelling approach used in this paper has demonstrated its usefulness to provide deeper understanding of physical mechanisms driving the barotropic wind-driven circulation in homogeneous bays where rotational and advection effects are small. This has been illustrated for various analytical test cases (infinite channel, rectangular basins) as well as for a realistic application (lagoon of Mururoa). It is worth stressing that all model results are subject to the limits of their underlying assumptions: a simplified dynamical balance and a simple but crude approximation of vertical exchange of momentum by a constant viscosity. However, despite these approximations, the simple model was shown to include enough physics to capture the essence of the role bathymetry in Mururoa.

Acknowledgements

We are deeply grateful to Benoit Tartinville for providing us with the bathymetry of Mururoa and to Susane Adcock, David Marshall and John Thuburn for their useful comments. Eric Deleersnijder and Jean-Marie Beckers are Research associates with the Belgian National Fund for Scientific Research (FNRS)

Appendix A

A.1. Geometrical property of depth moments

In this section, we derive a geometrical property, which states that the inversion depth is deeper than the mean depth,

$$H_* \equiv \frac{\overline{H^3}}{\overline{H^2}} \geqslant \bar{H}. \tag{A.1}$$

This is readily demonstrated by considering the following function:

$$F_P \equiv (H - \bar{H})^2 \overline{H^2} H + (H\bar{H} - \overline{H^2})^2 \bar{H} \tag{A.2}$$

which has a section-average of (where overbars refers to operator of Eq. (15))

$$\bar{F}_P \equiv \overline{H^2}(\overline{H^3} - \bar{H}\overline{H^2}). \tag{A.3}$$

The positivity of F_P (trivially verified since each term of F_P is positive) implies that $\overline{F_P} \geqslant 0$ which readily provides property of Eq. (A.1).

A.2. Upper and lower bounds of directional transport

In this section, we derive an upper and lower limit for the dimensionless directional transport per unit area defined in Eq. (28). To do this, let us define the following functions:

$$U'_{-}L \equiv \frac{1}{27} + \frac{1}{3}\left(\frac{H}{H_*} - 1\right) + \frac{15}{27}\left(\frac{H}{H_*} - 1\right)^2 + \frac{7}{27}\left(\frac{H}{H_*} - 1\right)^3 = \frac{7}{27}\frac{H^3}{H_*^3} - \frac{6}{27}\frac{H^2}{H_*^2}, \quad \text{(A.4)}$$

$$U'_{-}H \equiv \frac{1}{27} + \frac{1}{3}\left(\frac{H}{H_*} - 1\right) + \frac{19}{16}\left(\frac{H}{H_*} - 1\right)^2 + \frac{1}{2}\left(\frac{H}{H_*} - 1\right)^3. \quad \text{(A.5)}$$

Averaging these functions across the channel yields

$$U'_{-}L = \frac{1}{27}\frac{\overline{H^2}}{H_*^2}, \quad \text{(A.6)}$$

$$U'_{-}H = \frac{169}{432} - \frac{13}{24}\frac{\bar{H}}{H_*} + \frac{3}{16}\frac{\overline{H^2}}{H_*^2}. \quad \text{(A.7)}$$

It is readily seen that each term of Eqs. (A.4) and (A.5) are, respectively, geometrically inferior and superior to the expression of Eq. (27). This implies that $\bar{U}'_{-}L \leqslant \bar{U}'_{-} \leqslant \bar{U}'_{-}H$ which yields the following inequality:

$$\frac{\bar{U}'_{-}L}{S'^2} \leqslant q' \leqslant \frac{\bar{U}'_{-}H}{S'^2}. \quad \text{(A.8)}$$

By using Eq. (A.1) to bound the second term of Eq. (A.7) divided by S'^2, we finally obtain the upper and lower limits of q',

$$\frac{1}{27}\frac{\overline{H^2}}{\bar{H}^2} \leqslant q' \leqslant -\frac{13}{24} + \frac{169}{432}\left(\frac{\bar{H}}{H_*}\right)^{-2} + \frac{3}{16}\frac{\overline{H^2}}{\bar{H}^2}. \quad \text{(A.9)}$$

References

Black, K.P., 1993. The relative importance of local retention and inter-reef dispersal of the neutrally buoyant material on coral reefs. Coral Reefs 12, 43–53.

Blumberg, A.F., Mellor, G.L., 1987. A description of the three-dimensional coastal ocean circulation model. In: Heaps, N.S. (Ed.), Three-Dimensional Coastal Ocean Models. American Geophysical Union, Washington, DC, pp. 1–16.

Bourlat, Y., Millies-Lacroix, J.C., Nazard, R., 1995. Determination of plutonium radioactivity in Mururoa Lagoon water. Journal of Radioanalytical and Nuclear Chemistry 197, 393–414.

Bryan, K., 1969. A numerical method for the study of the circulation in the ocean. Journal of Computational Physics 4, 347–376.

Burchard, H., 1998. Presentation of a new numerical model for turbulent flow in estuaries. In: Babovic, V., Larsen, L.C. (Eds.), Hydroinformatics. Balkema, Rotterdam, pp. 41–48.

Csanady, G.T., 1973. Wind-Induced barotropic motions in long lakes. Journal of Physical Oceanography 3, 429–438.

Csanady, G.T., 1980. Longshore pressure gradients caused by off-shore wind. Journal of Geophysical Research 85, 1076–1084.

Davies, A.M., 1990. On the importance of time varying eddy viscosity in generating higher tidal harmonics. Journal of Geophysical Research 95, 20287–20312.

Davies, A.M., Jones, J.E., 1990. Application of a three dimensional turbulence energy model to the determination of tidal currents on the Northwest European shelf. Journal of Geophysical Research 95, 18143–18162.

Davies, A.M., Kwong, S.C.M., Flather, R.A., 2000. On determining the role of the wind wave turbulence and grid resolution upon computed storm driven currents. Continental Shelf Research 20, 1825–1888.

Deleersnijder, E., Tartinville, B., Rancher, J., 1997. A simple model of the tracer flux from the Mururoa lagoon to the Pacific. Applied Mathematics Letters 5, 13–17.

Glorioso, P.D., Davies, A.M., 1995. The influence of eddy viscosity formulation, bottom topography, and wind wave effects upon the circulation of a shallow bay. Journal of Physical Oceanography 25, 1243–1264.

Hearn, C.J., Hunter, J.R., Heron, H., 1987. The effects of a deep channel on the wind induced flushing of a shallow bay or harbor. Journal of Geophysical Research 92 (C4), 3913–3924.

Hunter, J.R., Hearn, C.J., 1987. Lateral and vertical variations in the wind-driven circulation in long, shallow lakes. Journal of Geophysical Research 92 (C12), 13106–13114.

Mellor, G.L., Yamada, T., 1982. Development of a turbulence closure models for geophysical fluid problems. Reviews of Geophysics and Space Physics 20, 851–875.

Rancher, J., 1995. Courantologie à proximité des flancs et devant les passes des atolls de Mururoa et Fangataufa. Technical report 01/SMSRB/NP. Service Mixte de surveillance Radiologique et Biologique de l'homme et l'environnement, unpublished.

Signell, R.P., Beardsley, R.C., Graber, H.C., Capatondi, A., 1990. Effects of wave-current interaction on wind-driven circulation in narrow, shallow embayments. Journal of Geophysical Research 95, 9671–9678.

Simons, T.J., 1980. Circulation models of lakes and inland seas. Bull. 203, Department of Fisheries and Ocean, Ottawa, Ontario, Canada, pp. 146.

Tartinville, B., 1998. Modélisation Tridimensionnelle de la Circulation Dans le Lagon de l'Atoll de Mururoa, Polynésie Française. Ph.D. Thesis, Catholic University of Louvain, Louvain-la-Neuve, Belgium, unpublished.

Tartinville, B., Deleersnijder, E., Rancher, J., 1997. The water residence time in the Mururoa atoll lagoon: sensitivity analysis of a three dimensional model. Coral Reefs 16, 193–203.